

Developments of 3-D Reconstruction Algorithms for ERT

P.A.T. Pinheiro, W.W. Loh and R.C. Waterfall

Process Tomography Unit,
Department of Electrical Engineering and Electronics, UMIST
P.O. Box 88, Manchester, M60 1QD, United Kingdom

Abstract - *Electrical resistance tomography (ERT), is an imaging tool for process and clinical applications, in which maps of the electric conductivity distribution of a body are formed from the current-to-voltage map of the body's surface. ERT is inherently a three-dimensional problem, as the current lines do not remain localised in a plane. The transposition of two-dimensional (2-D) ERT to three-dimensional (3-D) ERT is a challenging task and imposes significant increase in computational power demands and storage requirements. In this work, it is demonstrated that 3-D ERT is a viable off-line technique for use today and can be implemented using a low-cost Pentium powered PC. The 3-D image reconstruction algorithm implemented is based on the Newton's method in which optimal experiments are used for the reconstruction process. More importantly, the algorithm incorporates 3-D forward modelling, 3-D data collection and reconstruction. A 'fast' reconstruction algorithm is also implemented and yields a reduced set of equations, which has the advantage of no longer being ill conditioned at expense of a loss in the image resolution. The reconstruction algorithm was applied to a 2.7m³ mixing tank at plant scale and the resulting images analysed.*

Keywords : Finite element method, forward problem, inverse problem, 3-D tomography

1. INTRODUCTION

Delineation of the internal composition of, for example, pipelines and mixing vessels is the primary objective of process tomography. Electrical resistance tomography (ERT) offers a relatively low-cost route to determine, in a non-destructive manner, the dynamic state of such processes via sets of electrical impedance measurements taken from electrodes mounted onto the periphery of the vessel. The tomographs produced by this apparatus can be used to better understand the process kinetics and provide on-line control of the process to reduce energy consumption and increase product yield. This paper describes work performed by the authors in order to create a 3-D image reconstruction algorithm to produce quantitative images.

In this work, the reconstruction procedure is fully based on 3-D forward modelling, 3-D data collection and 3-D reconstruction. The algorithm implemented iteratively uses linear conductivity updates in conjunction with a general forward solver, thereby providing a non-linear algorithm.

2. QUANTITATIVE IMAGE RECONSTRUCTION

The inverse problem in electrical resistance tomography is a non-linear inverse one. The non-linearity arises due to the equipotential lines curving in a way which depends on the spatial conductivity distribution. In this work, the method used to solve the non-linear problem is to reduce it to an iterative procedure using the Newton's method. It is well known that it exhibits quadratic convergence for a non-singular derivative [[8]]. However, the method presented in this work delivers a convergence, which is an interpolation between the quadratic convergence of Newton, and that of the linear convergence of the steepest descent method.

The Newton-type process of a multi-iteration algorithm is performed in two stages. In the first stage, a numerical model is used to predict the voltage measurements that would be made on a region with a conductivity distribution, which is the best estimate, so far, of the spatial conductivity of the region being imaged. This stage is referred to as the forward problem. In the second stage, designated as the inverse problem, this best estimate spatial conductivity is updated in such a way to better predict the behaviour of the region being imaged.

2.1 The Forward Problem

In order to solve the forward problem in ERT, use of numerical methods are necessary since for an arbitrary conductivity distribution there is no analytical solution. The most commonly used technique to model this stage is the finite element method (FEM). The FEM discretises the region of interest into small elements with constant conductivity and the potential distribution is approximated using a polynomial basis to interpolate between specified nodal values. Therefore, a piece-wise homogeneous model is constructed. The FEM transforms the forward problem into a problem of solving a set of linear equations, which can be regarded as Ohm's law and Kirchoff's law combined:

$$\mathbf{Y} \cdot \Phi = \mathbf{C} \quad (1)$$

where \mathbf{Y} is a symmetric positive definite n by n conductance matrix (units: siemen), Φ is an n -dimensional vector which represents the potential (units: volt) at n discrete points and \mathbf{C} is also an n -dimensional vector which contains the applied current at the previous n discrete points (units: ampere).

The algorithm implemented for the solution of the system in Equation (1) is based upon Cholesky factorisation since it only performs one factorisation of the \mathbf{Y} matrix for different applied current boundary conditions \mathbf{C} employed in ERT. The Cholesky factorisation decomposes the conductance matrix \mathbf{Y} into a product of a lower triangular matrix \mathbf{L} whose transpose serves as the upper triangular matrix \mathbf{L}^T as follows:

$$\mathbf{Y} = \mathbf{L} \cdot \mathbf{L}^T \quad (2)$$

Then, the vector Φ is solved by forward ($\mathbf{L} \cdot \mathbf{x} = \mathbf{C}$) and backward ($\mathbf{L}^T \cdot \Phi = \mathbf{x}$) substitution.

The \mathbf{Y} matrix is sparse and therefore a suitable candidate for treatment with sparse matrix methods. In order to provide an indication as to how these numbering schemes affect the computation time to achieve a solution, the following schemes were applied to two cylindrical meshes comprising 1536 upright prismatic elements: Minimum Degree (MDG), Minimum Deficiency (MDF) and Nested Dissection (ND). One mesh was assembled using linear upright prismatic elements and the other mesh was composed of quadratic upright prismatic elements (see Figure 1). It should be noted that for this particular type of upright finite elements an analytical stiffness matrix can be computed and the interested reader is referred to Pinheiro *et al.* [11]. For a detailed explanation of these strategies and more results on other representative 2-D ERT meshes see elsewhere [3,[12]].

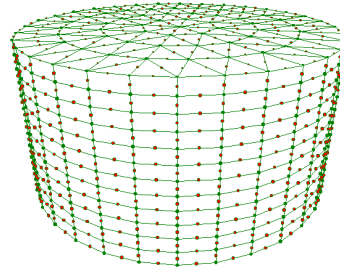


Figure 1. Three-dimensional cylindrical ERT mesh assembled using upright quadratic prismatic elements. To obtain a linear element mesh, the quadratic elements are simply replaced by the upright linear prismatic elements

The performance, with respect to speed, of the different re-numbering schemes are listed in Table 1. An operation count or flop is defined as a floating-point multiplication followed by an addition. All algorithms use the compressed storage scheme described by George and Liu [3].

Mesh	Stage	MDG	ND	MDF
1536 linear 1053 nodes	Factorisation	1.19	1.30	0.90
	Substitution	0.04	0.04	0.03
	Total	1.23	1.34	0.93
1536 quadratic 4729 nodes	Factorisation	59.28	40.74	21.31
	Substitution	0.56	0.48	0.36
	Total	59.84	41.22	21.67

Table 1 Computation time in seconds for solving the linear system of equations. All tests were performed on a 90 MHz Pentium PC. The 'C' code was compiled using the Power Pack DOS extender from Borland with the Borland C++ v.4.5 compiler.

The sparse techniques decrease the computation time by reducing the number of flops required to factorise the conductance matrix \mathbf{Y} . The reason being that trivial computations such as multiplication by zero are avoided.

2.2 The Inverse Problem

The method implemented defines a regularised solution of the inverse problem as a conductivity distribution, which minimises an objective function of the form,

$$e\left(\mathbf{s}^{(k)} + \Delta\mathbf{s}^{(k)}\right) = \left\| \mathbf{G}\left(\mathbf{s}^{(k)}\right) - \mathbf{G}_{ROI} + \mathbf{J}\left(\mathbf{s}^{(k)}\right) \cdot \Delta\mathbf{s}^{(k)} \right\|^2 + a \left\| \mathbf{D} \cdot \left(\mathbf{s}^{(k)} + \Delta\mathbf{s}^{(k)}\right) \right\|^2 \quad (3)$$

where $\| \cdot \|$ is the 2-norm, \mathbf{G}_{ROI} is the experimental measurement, $\mathbf{G}(\sigma^{(k)})$ is a general forward operator that maps the conductivity model to the experimental measurement model, $\mathbf{J}(\sigma^{(k)})$ is a

derivative matrix which is commonly referred to as Jacobian matrix, $\sigma^{(k)}$ is the present best conductivity estimate, $\Delta\sigma^{(k)}$ is the conductivity update, k is the iteration number, α is a positive number known as smoothness parameter and \mathbf{D} is a regularisation operator. The last term in Equation (3) involving the \mathbf{D} operator is often referred to as the roughness term. Upon applying the standard Gauss-Newton method to minimise the above objective function, the resulting equation for an iterative solution is given by [15],

$$\mathbf{s}^{(k+1)} = \mathbf{s}^{(k)} - \left(\mathbf{J}^T \bullet \mathbf{J} + \alpha \mathbf{D}^T \bullet \mathbf{D} + \mathbf{m} \right)^{-1} \bullet \left[\mathbf{J}^T \bullet \left(\mathbf{G}(\mathbf{s}^{(k)}) - \mathbf{G}_{ROI} \right) + \alpha \mathbf{D}^T \bullet \mathbf{D} \bullet \mathbf{s}^{(k)} \right] \quad (4)$$

where for simplicity $\mathbf{J}^T(\sigma^{(k)})$ was replaced by \mathbf{J}^T . This type of inversion is often referred to as smoothness-constrained inversion or Occam's inversion in the geophysical literature and there are different variations according to the choice of the regularisation operator \mathbf{D} [1],[15]. The idea underpinning this type of inversion is that, rather than fitting the experimental data as well as possible, which maximises the roughness of the conductivity distribution, the smoothest conductivity distribution that fits the data to within expected tolerance is sought.

The regularisation operator \mathbf{D} was chosen using the following procedure:

*Input a smoothness radius R.
For i=1 to number elements in the mesh
Assign $D_{i,i} = -1$.
Obtain all elements (k) whose centre point distances are equal to or less than R, and assign to those elements a weight equal to $1/n$ (i.e. $D_{i,k} = -1/n$) where n is the number of elements inside radius R excluding the reference element i. For all others assign a zero weight.
Next i*

2.3 Reconstruction algorithm

The process can be summarised as follows: firstly, data is acquired from the ROI using the diagonal data collection protocol [2], which is only performed once, enabling the computation of a transfer resistance matrix which represents all the information that can be extracted via the electrodes; an identical procedure is repeated for an initial case of a homogeneous spatial conductivity distribution in the numerical model; secondly, the difference between the two previous matrices is computed in order to find the optimal experiments, which are calculated using the singular value decomposition (SVD) procedure; thirdly, the Jacobian information is computed based on the optimal experiments and

the current conductivity in the numerical model; lastly, a conductivity update is computed using a regularised Newton method. This procedure is iteratively applied to the numerical model until there is evidence that no lower minimum can be found in the objective function.

2.3.1 Computation of the transfer resistance matrix $\mathbf{R}(\sigma)$.

If one models the L -electrode ERT system into an L -terminal network in which the circuit ground is taken as reference, then by Ohm's law, the relation among voltage \mathbf{V} , current \mathbf{I} and resistance $\mathbf{R}(\sigma)$ is,

$$\mathbf{V} = \mathbf{R}(\mathbf{s}) \bullet \mathbf{I} \quad (5)$$

where \mathbf{V} and \mathbf{I} are both L -dimensional vectors whose elements are the potential and currents on the electrodes, respectively, and element R_{ij} denotes transfer resistance between terminal i and j . The region being imaged has no current sources and therefore, the transfer resistance matrix $\mathbf{R}(\sigma)$ is symmetrical, namely $R_{ij} = R_{ji}$. The continuous medium also ensures that none of the terminals are isolated from the rest of the network. Hence, the matrix is indefinite and its rank is at most $L-1$. Consequently, one can uniquely determine all elements of the matrix $\mathbf{R}(\sigma)$ by injecting a set of $L-1$ independent current bases and measuring the resulting voltages.

2.3.2 Computation of optimal currents and optimal measurements

Paulson *et al.* [[10]] defined an experiment in ERT as a measurement of a component of the difference between the voltage pattern induced on the surface of the region being imaged and that predicted by a numerical model by the application of a current pattern to the surface. An experimental measurement E_{ij} yields a single number, that is,

$$E_{ij} = \mathbf{M}_i^T \bullet (\mathbf{R}_{FEM} - \mathbf{R}_{ROI}) \bullet \mathbf{I}_j \quad (6)$$

where \mathbf{M}_i^T is an L -dimensional vector which comprises a 'weight' to give to each measurement commonly termed a measurement pattern and \mathbf{I}_j is an L -dimensional vector with the current delivered to each electrode. The matrices \mathbf{R}_{FEM} and \mathbf{R}_{ROI} are the transfer resistance matrices for the numerical model and that of the region of interest, respectively. Therefore, one wishes to find current patterns and measurement patterns that maximise E_{ij} , that is,

$$\max_{\substack{\mathbf{I}_j: \|\mathbf{I}_j\|=1 \\ \mathbf{M}_i: \|\mathbf{M}_i\|=1}} \|\mathbf{E}_{ij}\| \quad (7)$$

where the norm is the Euclidean norm, also called a '2-norm'. The current and measurement patterns are of unit norm since the voltages scale with the current, and larger experimental measurements can always be found by uniformly increasing the magnitude of the injection currents and/or measurement patterns. The problem of maximising E_{ij} is an eigenvalue problem for the matrix $\mathbf{R}_{FEM} - \mathbf{R}_{ROI}$, which can be solved numerically using the standard singular value decomposition (SVD) techniques [[14]]. Consequently, the optimal experimental measurement E_{ij} is given by [[9]],

$$\begin{aligned} E_{ij} &= \mathbf{U}_i^T \cdot (\mathbf{R}_{FEM} - \mathbf{R}_{ROI}) \cdot \mathbf{V}_j \\ &= \mathbf{U}_i^T \cdot \mathbf{I}_j \cdot \mathbf{V}_j = \mathbf{I}_i \cdot \mathbf{d}_{ij} \end{aligned} \quad (8)$$

where $\delta_{ij} = 1$ for $i=j$ and $\delta_{ij} = 0$ for $i \neq j$, λ_i are the singular values, \mathbf{M}_i was chosen to be the i^{th} column in matrix \mathbf{U} (i.e. left orthonormal matrix) and \mathbf{J}_i was selected as the i^{th} column in matrix \mathbf{V} (i.e. right orthonormal matrix). The analysis shows that the best experimental measurement that can be made is E_{11} , the next best is E_{22} , etc. All E_{ij} with $i \neq j$ are zero. These patterns are optimal on the basis that they maximise the voltage measurements in the mean-square sense between the region being imaged and that of the numerical model. This is a crucial point since experimental measurements, which are small when compared to the background noise, render poor information on which to base the reconstruction process. As a consequence of the matrix symmetry and the use of the reciprocity theorem [[4]], the number of independent measurements is readily computed as being equal to $L(L-1)/2$. Therefore, all the information is contained in experiments E_{ij} with $i = 1$ to $L-1$, $j = i$ to $L-1$. If the reconstruction algorithm is based on these experiments, then the conductivity update will be such that it minimises the Frobenius norm of the difference in the transfer resistance matrices of the numerical model and the region being imaged.

2.4 Fast reconstruction

The authors also implemented the POMPUS3D algorithm devised by Paulson [[9]]. The method is also based on the use of optimal currents and measurements. The major advantage of the algorithm is the reduction in computational cost in calculating the conductivity update. This is accomplished by not including the experimental measurements $E_{ij} : i \neq j$. Therefore, the conductivity update is computed as,

$$\Delta\sigma = \mathbf{J}_R^T \cdot (\mathbf{J}_R \cdot \mathbf{J}_R^T)^{-1} \cdot \mathbf{E}_R \quad (9)$$

where $\mathbf{J}_R^T = [\mathbf{J}_{11}^{*T}, \mathbf{J}_{22}^{*T}, \dots, \mathbf{J}_{L-1,L-1}^{*T}]$, $\mathbf{E}_R^T = [E_{11}, E_{22}, \dots, E_{L-1,L-1}]$. Therefore, in order to compute the conductivity update, one only needs to solve an $(L-1) \times (L-1)$ linear system of equations as given in Equation (9) which is no longer ill conditioned. Tests performed for three-dimensional problems revealed that its condition number never exceeded 3.0×10^3 .

2.5 Computation Effort

In Table 2, the time for a single iteration for the three-dimensional algorithm is given. From this, it can be seen that the standard three-dimensional reconstruction is excessively time consuming whether one uses either a linear or a quadratic mesh. The most time consuming stage is the computation of the Jacobian matrix \mathbf{J} and the associated matrix $\mathbf{J}^T\mathbf{J}$ which take approximately 86% of the overall iteration time. The computation of the matrix $\mathbf{J}^T\mathbf{J}$ requires approximately 2.3 GFlops, while for the Jacobian matrix \mathbf{J} , 743 MFlops and 130 MFlops are necessary for the quadratic and linear mesh, respectively. A 'Flop' is defined as a multiplication followed by an addition. This is the main reason why there are no significant differences in computing times using linear or quadratic meshes. Clearly, this result confirms that, for the large amount of Flops involved, real-time three-dimensional imaging is only possible using a super computer. However, if one is willing to use the POMPUS3D algorithm, the computing times are reduced by at least one order of magnitude. In the POMPUS3D, the forward problem plays an important role as the computation of matrices \mathbf{J} and $\mathbf{J}^T\mathbf{J}$ take 39% and 22% of the overall iteration time for the linear and quadratic mesh, respectively. An alternative approach to improve computing times is to build dedicated parallel computing hardware to handle the computation of the matrix $\mathbf{J}^T\mathbf{J}$. Loh [[7]] described such an architecture referred to as a 3-dimensional array processor (3DAP). The system comprised 4 low-cost (~£50) Texas Instruments TMS 320C31 digital signal processors (DSPs) and yielded a sustainable performance of 145.6 MFlop/s.

TASK	1536 linear		1536 quadratic	
	Recon	Fast	Recon	Fast
R_{FEM}	4.6	4.6	51.4	51.4
Opt. Experiments	5.0	5.0	32.5	32.5
$J, J^T J, J^T E$	1130.5	6.2	1561.2	24.7
Conductivity update	180.7	<0.05	18.7	<0.05
TOTAL	1320.8	15.8	1825.8	108.6

Table 2 Time in seconds for a single iteration of the three-dimensional reconstruction algorithm for two different meshes: 1536 linear upright prismatic elements and 1053 nodes; 1536 quadratic upright prismatic elements and 4729 nodes. The 'C++' code was compiled using the Power Pack v.1.0 DOS extender from Borland with the Borland C++ v.4.5 compiler and the resulting executable file run on a 90 MHz Pentium PC.

3. EXPERIMENTAL RESULTS

As reported elsewhere [5], a 2.7m³ semi-tech scale mixing vessel located in the Department of Chemical Engineering Pilot Plant at UMIST was retrofitted with an 8-plane sensor array. Each sensor plane consists of PVC trunking to which are affixed 16 equally spaced 10 x 3.8 cm (width/height) stainless steel electrodes. A diagram depicting the physical dimensions of the mixing vessel is shown in Figure 2. In the following sub-sections, the authors demonstrate the feasibility of using 3-D imaging electrical resistance tomography in the mixing vessel described above.

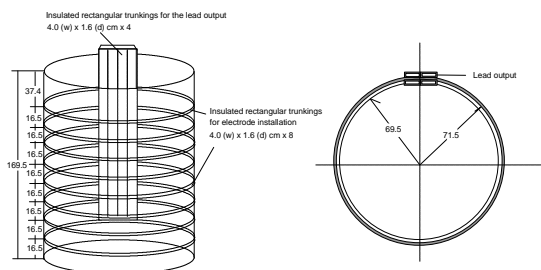


Figure 2. Schematic view of the mixing tank. Each of the eight rings of electrodes contains 16 electrodes whose dimensions are 10 cm (w) x 3.8 cm (h).

3.1 Object Detection

The experiment consisted of placing three plastic bottles ($\sigma > 10^{-9}$ S cm⁻¹ @ 20°C) acting as phantoms in the mixing vessel, which was filled with "mains" tap water ($\sigma \approx 0.1$ mS cm⁻¹ @ 20°C) as depicted in Figure 3.



Figure 3. Photographic view of the 2.7 m³ mixing tank filled with water together with three plastic bottles. The dimensions of the plastic bottles are 19 cm diameter and 27 cm high.

The data was collected using only the even numbered rings of electrodes (*i.e.* 4 electrode planes) where ring number 1 is the top ring in the mixing tank. The reason for using only 4 of the 8 planes is that presently the Mark 2a UMIST DAS [13] is not able to drive the 8 planes simultaneously. A 19.5 kHz, 5 mA peak-to-peak sinusoidal current was used to excite the sensors using the diagonal data collection. The 3969 voltage measurements took approximately 4 secs to acquire using the Mark 2a UMIST Data Acquisition System. At present, this lengthy data acquisition procedure is the main limitation to observe dynamic states. Therefore, one can only visualise static or pseudo-static situations. The image was then reconstructed using a three-dimensional mesh assembled using 1536 quadratic upright prismatic elements (see Figure 1). In Figure 4, the interpolated reconstructed image is presented. From Figure 4, it is evident that the algorithms are able to successfully locate the bottles. This is not surprising since the bottles impose an almost infinite conductivity contrast. However, to quantify such large conductivity changes is exceedingly difficult. Shi *et al.* [6] performed a numerical study using the boundary element method (BEM) and they reported that the boundary potential difference is more sensitive to small changes in conductivity and that this sensitivity ($\Delta v/\Delta\sigma$) approaches zero when the conductivity changes are very large. This fact explains the limited conductivity range for the Occam-regularised images of 8102-26852Ωcm, respectively. Moreover, the use of regularised inversion further 'damps' the reconstructed conductivity values. A region of low resistivity is also observed in Figure 4 (a), which is the result of the metallic impeller. The POMPUS3D algorithm, although very intensive, exhibits worse convergence properties and delivers a conductivity range which is limited when compared with the standard reconstruction. Furthermore, the low resolution is apparent in the reconstructed objects. However, if one intends to

produce low resolution images in a moderate time, the POMPUS3D is an attractive alternative.

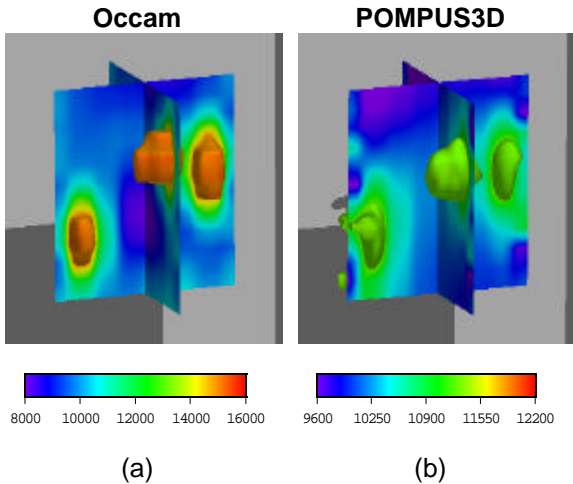


Figure 4 Three-dimensional conductivity distributions for the case displayed in. The conductivity values ranged from 8102-26852 Ωcm for the Occam's regularisation and 8891-12188 Ωcm for the Fast Recon. The isosurfaces correspond to a value of 15000 Ωcm for the Occam regularisation, while for the Fast Recon algorithm, this value corresponds to 11250 Ωcm .

3.2 Imaging an Air-Core Vortex in an Unbaffled Stirred Vessel

An air-core vortex is present inside a stirred vessel whenever it is operated without baffles. In order to produce an air-core vortex, a six-bladed Rushton turbine was fitted into the mixing tank and operated at 140rpm. Figure 5 shows the effect. The baffles at the periphery create mini-vortices thereby improving the mixing kinetics of the vessel. The vessel was deliberately operated without baffles in this experiment to create a central air-core vortex. It was hoped that ERT could detect the air-core vortex ($\sigma \approx 0 \text{ mS cm}^{-1}$) and characterise its shape.

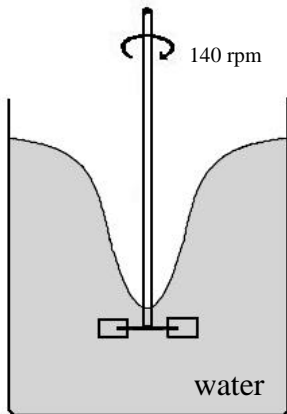


Figure 5 Cross-section view along the vertical axis of the air-core vortex.

The reconstructed pseudo-stationary air-core vortex is shown in Figure 6 where a 19.5 kHz, 5

mA peak-to-peak sinusoidal current was used to excite the sensors using the diagonal data collection protocol. The comparative analysis of the three images reveals that the standard Levenberg-Marquardt regularisation [2] appears to produce a more representative image of the air-core witnessed during the experiment, which approximates an inverted 'bell'-shaped profile. Although, all of the algorithms readily identify the existence of an air-core vortex, they clearly fail to characterise its shape, particularly for the Occam's inversion. This outcome is probably due to two factors: the water level in the mixing tank rises when the air-core is present and the voxels on the top and bottom part of the vessel are the least determined by the data. However, these points require further investigation. One must also bear in mind that the central region is the most difficult region to image. The conductivity range of the reconstructed images is once again limited: 7,666-84,097 Ωcm for Occam's regularisation and 6,492-20,887 Ωcm for the Levenberg-Marquardt regularisation. This fact is due to the problem associated with imaging large conductivity changes as explained in the previous sub-section. The high peak conductivity value of 84,097 Ωcm for the Occam's regularisation is the consequence of assigning the wrong shape to the air-core, which is compensated by an excessive conductivity value at the centre of the cylindrical mixing tank. The Fast Recon, although producing relative small conductivity values when compared to the standard Recon, delivers a comparatively better air-core shape than that of Occam's regularisation requiring substantially less computing power. Therefore, the Occam's regularisation tends to penalise conductivity changes near the top of the mixing tank. For visualising an air-core vortex, since one has *a priori* information about a typical air-core shape, maybe in the future, a reconstruction algorithm can incorporate this information in the conductivity update. Finally, a brief remark about the operating environment should be made. The motor, which drives the impeller, is a significant source of electrical noise via radio frequency interference into the DAS and electric coupling into the electrodes. In addition, the mixing tank physically vibrates causing the cylindrical vessel to distort due to the water agitation, which undoubtedly affects the overall quality of the acquired data.

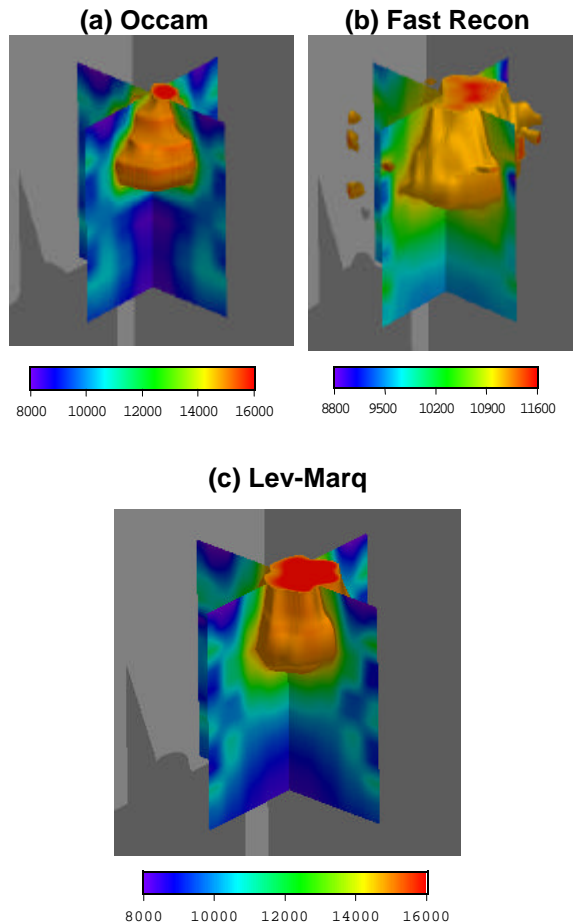


Figure 6 Three-dimensional conductivity distributions for the case displayed in Figure 5. The resistivity values ranged from 7666-84097 Ωcm for the Occam's regularisation, 6492-20887 Ωcm for the Levenberg-Marquardt regularisation, and 7869-12373 Ωcm for the Fast Recon. The isosurfaces correspond to a value of 15000 Ωcm for the Occam and Levenberg-Marquardt regularisation, while for the Fast Recon algorithm, this value corresponds to 11250 Ωcm .

4. CONCLUSION

Electrical resistance tomography is inherently a three-dimensional problem. The transposition of two-dimensional ERT to three-dimensional ERT is a challenging task and imposes significant increase computational power demands and storage requirements. Although two-dimensional real-time on-line quantitative imaging is possible today with conventional PCs, the same cannot be claimed for three-dimensional imaging unless a super computer is used. However, it has been demonstrated that three-dimensional ERT is a viable off-line technique for use today and can be implemented using a low-cost Pentium powered PC.

ACKNOWLEDGEMENT

P.A.T. Pinheiro gratefully acknowledges the financial support of the Portuguese PRAXIS XXI (JNICT) Programme [Fellowship ref. BD/2957/94]. W.W. Loh would like to acknowledge the financial support given by Engineering and Physical Sciences Research Council [ESPRC GR/K59088]. The authors would like to thank Dr. Mi Wang for help in setting up the mixing tank to conduct the experiments.

REFERENCES

- [1] DeGroot Hedlin C. & Constable S. "Occam's inversion to generate smooth 2-D models" *Geophysics*, vol.55, no.12, pp1613-1624, 1990
- [2] Pinheiro PAT "A 3-D Reconstruction Algorithm for ERT" PhD Thesis, UMIST, 1998.
- [3] George A., Liu J.W. "Computer Solution of Large Sparse Positive Definite Systems", 1981, (Prentice-Hall series in Mathematics).
- [4] Geselowitz D.B. "An Application of Electrocardiographic Lead Theory to Impedance Plethysmography" *IEEE Transactions on Biomedical Engineering*, 1971, **18** pp.38-41.
- [5] Mann R, Wang M, Dickin FJ, et al. "Resistance tomography imaging of stirred vessel mixing at plant scale" Benkreira H (ed) *Fluid Mixing 5*, Inst. Chem. Eng. Symp. Ser No 140, 1995
- [6] Shi Y, Margili PM, Dai WW, Gramie M & Morucci JP. "Application of the BEM to the study of boundary potentials in EIT" *Clin Phys Physiol Meas*, 1992, 13, suppl A, pp139-143
- [7] Loh W.W., "An Array Processor for Real-Time Reconstruction of Tomographic Images", MSc Thesis, Department of Electronics and Electrical Engineering, UMIST, 1995.
- [8] Ortega J.M. and Rheinboldt, "*Iterative Solution of Nonlinear Equations in Several Variables*", Academic Press, 1970.
- [9] Paulson K., "Parallel Algorithms for Three-Dimensional Electrical Impedance Tomography" Ph.D. Thesis, Oxford Brookes University, November 1992.
- [10] Paulson K., Lionheart W. and Pidcock M., "Fast, non-linear Inversion for Electrical Impedance Tomography", *Image and Vision Computing*, August 1994, **12** (6) pp. 367-373.

- [11] Pinheiro P.A.T., Dickin F.J. and James A.E., "Analytical Stiffness Matrix for the First and Second Order Upright Triangular Prismatic Elements" *Communications in Numerical Methods in Engineering*, 1997, **13** pp. 467-473.
- [12] Pinheiro, P.A.T. and Dickin F.J., "Sparse Matrix Methods for Use in Electrical Impedance Tomography", *International Journal Numerical Methods in Engineering*, 1997, **40** (3) pp. 439-451.
- [13] Pinheiro P.A.T., Loh W.W. and Dickin F.J., "Smoothness-Constrained Inversion for Two-Dimensional Electrical Resistance Tomography", *Meas.Sci.Technol.*, 1997. **8** pp. 293-302.
- [14] Press W., Teukolsky S., Vetterling W. and Flannery B., *Numerical Recipes in C*, 2nd edition, Cambridge University Press, 1992.
- [15] Zhang J., Rodi W., Mackie R.L. and Shi W., "Regularisation in 3-D DC Resistivity Tomography" *Society for the Application of Geophysics to Environmental and Engineering Problems*, Keystone, Colorado, pp. 687-694, 1996.